polymers

MDPI

Article

Strontium Aluminate-Based Long Afterglow PP Composites: Phosphorescence, Thermal, and Mechanical Characteristics

Anesh Manjaly Poulose [1,*], Arfat Anis [1,*], Hamid Shaikh [1], Abdullah Alhamidi [1], Nadavala Siva Kumar [2], Ahmed Yagoub Elnour [1] and Saeed M. Al-Zahrani [1]

[1] SABIC Polymer Research Center, Department of Chemical Engineering, King Saud University, Riyadh 11421, Saudi Arabia; hamshaikh@ksu.edu.sa (H.S.); AKFHK90@hotmail.com (A.A.); aelnour@ksu.edu.sa (A.Y.E.); szahrani@ksu.edu.sa (S.M.A.-Z.)

[2] Department of Chemical Engineering, King Saud University, Riyadh 11421, Saudi Arabia; snadavala@ksu.edu.sa

* Correspondence: apoulose@ksu.edu.sa (A.M.P.); aarfat@ksu.edu.sa (A.A.)

Abstract: A tremendous potential has been observed in the designing of long afterglow materials for sensing, bioimaging, and encryption applications. In this study, two different strontium aluminate-based luminescent materials; $SrAl_2O_4$: Eu, Dy (S_1), and $Sr_4Al_{14}O_{25}$: Eu, Dy (S_2) were melt-mixed with polypropylene (PP) matrix, and the phosphorescence properties were evaluated. After excitation at 320 nm, the PP/S_1 composite exhibited a green emission and the PP/S_2 generated a blue emission at 520 nm and 495 nm, respectively. The emission spectra intensity increased by increasing the content of these luminescent fillers. The attenuated total reflection-Fourier transform infrared (ATR-FTIR) experiments show that no chemical reaction occurred during the melt-mixing process. The differential scanning calorimetry (DSC) results revealed that the total crystallinity of the composites reduced by increasing the amount of the fillers; however, no changes in the temperature of melting (Tm) and crystallization (Tc) of PP were observed. Both fillers improved the impact strength of the composites, but the tensile strength (TS) and modulus (TM) decreased. Poly (ethylene glycol) dimethyl ether (P) plasticizer was used to improve the filler-matrix interaction and its dispersion; nevertheless, it adversely affected the intensity of the luminescence emissions.

Keywords: long afterglow PP composites; plasticizer; thermal; mechanical

Citation: Poulose, A.M.; Anis, A.; Shaikh, H.; Alhamidi, A.; Siva Kumar, N.; Elnour, A.Y.; Al-Zahrani, S.M. Strontium Aluminate-Based Long Afterglow PP Composites: Phosphorescence, Thermal, and Mechanical Characteristics. *Polymers* **2021**, *13*, 1373. https://doi.org/10.3390/polym13091373

Academic Editor: Swarup Roy

Received: 1 April 2021
Accepted: 21 April 2021
Published: 22 April 2021

1. Introduction

Luminescent materials emit light, especially in the visible region. When a material continuously emits visible light for longer time (hours) after stopping the radiating source (visible, UV, X-ray, or gamma-ray radiation), a persistence of luminescence or phosphorescence is observed [1]. The first-generation phosphors were Cu or Mn-doped ZnS-based materials (green emission at 530 nm) [2,3]. These materials have been exploited in catalysts and optoelectronic devices. However, their functions are limited because of their low brightness and short afterglow time, and chemical instability in the presence of moisture and CO_2.

A new luminescence era started with the detection of rare-earth-doped phosphors. The first batch of modern luminescent materials was the rare-earth (R^{3+}) and Eu^{2+} doped alkaline-earth aluminates (MAl_2O_4:Eu^{2+}, R^{3+}; M = Ca, Sr, or Ba) [4–9]. The Eu^{2+} doped phosphor exhibits a bluish-green luminescence, and the glowing time can be enhanced by adding rare-earth ions, such as neodymium (Nd) or dysprosium (Dy) (e.g., $SrAl_xO_y$: Eu^{2+}, Dy^{3+}), or by adding Al_2O_3 [4,10]. These phosphors have attracted much attention because of their long phosphorescence, greater stability (i.e., moisture and photo-stability), and high quantum efficiency compared with sulfide-based phosphors [9,11,12]. These materials can obtain radiation energy from solar light, remaining photo-luminescent for long periods of time (12–20 h) [13,14]. The luminescent properties of these phosphors allowed their

commercial acceptance because of the suitable usage in fluorescent lamps, glowing paints for highways buildings and airports, cathode ray tubes, plasma displays, textile, ceramic area, nighttime clocks, safety displays, among others. Significant growth in the use of these phosphors was observed in optoelectronics, telecommunications, optically active commercial products, and biomedical and way-finding systems [15–17].

Recently, various phases of strontium aluminates with rare-earth-doped were developed, such as $SrAl_2O_4$:Eu^{2+}, $Sr_2Al_{l6}O_{11}$:Eu^{2+}, $Sr_4Al_{14}O_{25}$:Eu^{2+}, $SrAl_{12}O_{19}$:Ce^{3+}, $SrAl_{12}O_{19}$:Pr^{3+}, and $Sr_4Al_{14}O_{25}$:Sm^{2+} [18–21]. The wavelength of the emitted visible light is decided by the crystalline phase structure of the resultant strontium aluminate [22,23]. Among the different $SrAl_xO_y$: Eu^{2+}, Dy^{3+} phosphors reported, $Sr_4Al_{14}O_{25}$: Eu, Dy, and $SrAl_2O_4$: Eu, Dy have exhibited the strongest potential for long phosphorescence and are commercially available [8,21,24]. Different synthesis techniques such as solid-state reactions [14,20,25], sol-gel method [11,24,26], combustion method [27], solvothermal method [28], chemical precipitation [29], microwave processing, and hydrothermal reaction [30] have been developed. These synthesis methods are often complex and require high temperatures for long-duration phosphorescence materials [31]. A mechanism for luminescence persistence was proposed for $SrAl_2O_4$:Eu^{2+}, Dy^{3+} and has been implied to explain the luminescence in several Dy^{3+} and Eu^{2+} co-doped silicates and aluminates. The mechanism is related to the thermally activated release of a hole from Eu^{2+} in its excited 5d state to the valence band, in which it is then trapped by Dy^{3+}. Luminescence is generated when the excited electron relaxes back to the ground state of Eu^{2+} [10,32]. The detailed mechanism of the process has been described [15]. However, $SrAl_xO_y$: Eu^{2+}, Dy^{3+} phosphors are not exempt from gradual luminescence decay due to their affinity towards moisture. Various encapsulation procedures have been described for gaining stable phosphor, such as Al_2O_3 [33], SrF_2 coating [34], phosphoric acid [35], organic ligands [36], amino-functionalized [37], among others, have been implied and reported. These processes are complicated, require elaborate equipment, and inversely affect the luminescence output. The easy and inexpensive method reported in the literature to prolong the afterglow properties of $SrAl_xO_y$: Eu, Dy is the encapsulation within a polymer matrix, which acts as an insulator for moisture. This process enables the composites to exhibit better chemical stability, good physical properties and can be processed very easily [38–45]. In this study, two different strontium aluminate materials doped with Eu, Dy were incorporated in the selected poly(propylene) matrix, and the phosphorescent characteristics of the resultant composites were studied in detail. Moreover, a known plasticizer poly (ethylene glycol) dimethyl ether (P) was used to enhance the phosphor dispersion in the PP matrix, and also to evaluate its effect on the phosphorescence emission. The characterization studies on these composites provide valuable information on the fabrication of polymer-based luminescent films.

2. Materials and Methods

2.1. Materials

Poly(propylene) (TASNEE PP H4120) was provided by TASNEE with a density of 0.9 g/cm^3. It has a melt flow rate (MFR) of 12 g/10 min (ISO 1133). The strontium aluminate phosphors, $SrAl_2O_4$: Eu, Dy (Mw = 209.11 g/mol) (S_1) and $Sr_4Al_{14}O_{25}$: Eu, Dy (1139.55 g/mol) (S_2), were supplied by Sigma Aldrich. The plasticizer employed in this study was poly (ethylene glycol) dimethyl ether (P) purchased from Aldrich Company having a number average molecular weight of Mn 1000.

2.2. Methods

2.2.1. Preparation of the Composites

Different weight percentages of phosphors (1, 3, 5, and 10) were melt-mixed with the PP matrix in a Polylab QC (Brabender mixer) for a mixing period of 3 min at a temperature of 190–200 °C at 40 rpm. Thin films of 0.5 mm average thickness were made using COLLIN Press, Germany for the phosphorescence measurements.

2.2.2. Characterization of the Composites

Phosphorescence measurements

The phosphorescence tests were carried out in a Fluorescence Spectrophotometer (Agilent Technologies, Santa Clara, CA, USA) using a Xe ultraviolet (UV) lamp. The emission spectra were collected at the wavelength of excitation 320 nm.

Scanning Electron Microscope (SEM)

The morphological and elemental analyses were performed in a JEOL JSM-6360A, Japan SEM model, with energy-dispersive X-ray spectroscopy (EDS) facility. A thin cut surface of the composite was prepared for the analyses. The gold coating for these samples is performed in an auto fine coater (JFC/1600) for 30 s. The coating with gold was carried out to prevent the effect of charging and to improve the quality of the image.

Attenuated Total Reflection-Fourier Transform Infrared Spectroscopy (ATR-FTIR)

ATR-FTIR tests were performed in a Thermo-Scientific Nicolet iN10 FTIR model with germanium micro-tip attachment (400–4000 cm^{-1}).

Differential Scanning Calorimetry (DSC)

DSC tests were done in Shimadzu DSC-60A model. Approximately 6–10 mg of sample were taken in an aluminum pan and is heated from 30 °C to 220 °C at a ramp of 10 °C/min with 4 min holding time.

The percent crystallinity was evaluated as follows

$$X_c(\%) = \frac{\Delta H_m}{(1-\Phi)\Delta H_m^0} \times 100$$

where (Φ) is the filler weight fraction in the composites, (ΔH_m) is the melting enthalpy, and ($\Delta H^0{}_m$) is the melting enthalpy of 100% crystalline PP, and was reported as 207 J/g [46].

X-Ray Diffraction (XRD)

The crystalline studies were performed in a wide-angle XRD (Bruker D8 advance). The diffractometer was endowed with a wide-angle goniometer attached to a sealed-tube Cu-Kα radiation source (λ = 1.54056 Å). The scanning was done in the 2θ range of 5° to 50° at 5°/min in the reflection mode.

Thermo-gravimetric analysis (TGA)

TGA was done in a Shimadzu DTG-60H model. For the analysis, 10 ± 1.5 mg of the samples were maintained in an aluminum pan and is heated to a temperature of 600 °C (inert atmosphere) with a heating rate of 20 °C/min; and the loss in weight was monitored.

Mechanical properties

The standard tensile testing specimens (ASTM Type1, Dumb-bell shaped) were prepared using a DSM Xplore, Netherlands (12 cm^3, microinjection molding). The mold was maintained at room temperature and at a pressure of 6 bar. Tensile testing was performed in Hounsfield H100 KS model UTM (ASTM D638), and the mean of five test results was reported.

3. Results

3.1. DSC and ATR-FTIR Data

The DSC data for the PP and its composites are displayed in Tables 1 and 2. The presence of both S_1 and S_2 did not considerably affect the temperature of melting (T_m) and crystallization (T_c) of the composites, demonstrating that the PP was not interacting chemically with S_1 and S_2 and the mixing process was purely physical. Additionally, the FTIR spectra also support this observation as PP, PP/10S_1, PP/10S_2, and PP/10S_1/5P have similar FTIR spectra, in which no new peaks were observed nor either peaks diminished (Figure 1). This observation confirms the absence of chemical reactions between both S_1 and S_2 and PP. The sharp peaks at 2900 cm^{-1} were due to the asymmetrical CH_2 bending and the peaks at 1450 cm^{-1} and 1380 cm^{-1} were assigned to the symmetrical CH_3 bending and asymmetrical CH_3 bending, respectively, of PP [47].

Table 1. DSC data of PP, PP/S_1, and plasticized composites.

Material	T_c (°C)	T_m (°C)	ΔH_m (J/g)	X_c (%)
PP	121.9	164.6	87.0	42.0
PP/$1S_1$	122.6	165.7	83.8	40.5
PP/$3S_1$	122.7	164.5	83.2	40.2
PP/$5S_1$	122.5	164.1	83.3	40.2
PP/$10S_1$	122.9	164.2	83.8	40.5
PP/$10S_1$/2.5P	122.0	164.0	82.5	39.9
PP$10S_1$/5P	121.6	163.9	76.6	37.0

Table 2. DSC data of PP and PP/S_2 composites.

Material	T_c (°C)	T_m (°C)	ΔH_m (J/g)	X_c (%)
PP	121.9	164.6	87.0	42.0
PP/$1S_2$	120.9	163.5	74.9	36.2
PP/$3S_2$	120.0	164.4	71.4	34.5
PP/$5S_2$	120.1	164.6	68.6	33.1
PP/$10S_2$	120.7	164.9	66.9	32.3

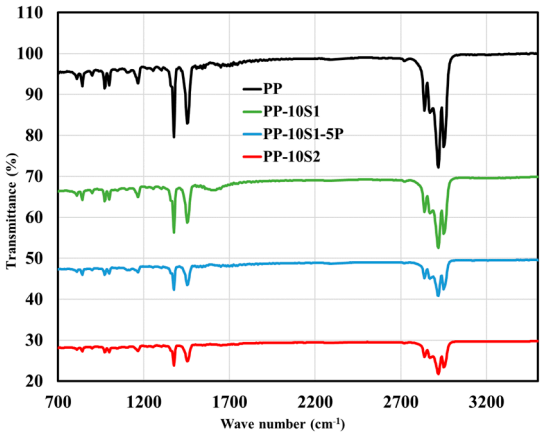

Figure 1. ATR-FTIR spectra of PP, PP/$10S_1$, PP/$10S_2$, and PP/$10S_1$/5P.

Conversely, the crystallinity of the composites decreased by increasing the S_1 and S_2 contents. The crystallinity decrease was more pronounced in S_2 because of the bulky chemical structure of S_2 compared with S_1, and in turn, restricts the PP chains mobility; thus, decreasing the crystallinity values [48]. The incorporation of the plasticizer in the composites led to a further reduction in the crystallinity percentage of the composites, as shown in Table 1.

3.2. X-ray Diffraction Studies of PP, PP/10S_1, PP/10S_2, and PP/10S_1/5P

Figure 2 illustrates the XRD patterns of neat PP, PP/$10S_1$, PP/$10S_2$, and PP/$10S_1$/5P. All composites show the characteristics diffraction peaks of α-PP, i.e., (110), (040), (130), and (111) [49]. Hence it was clear the absence of chemical reaction between PP and S_1, S_2 fillers, or the plasticizer. The (020) peak at 20°; (−211), (220), (211) peaks at 30°, and (031) peaks at 35° are the characteristics diffraction peaks of S_1 [39], and S_2 shows characteristics orthorhombic crystal structure with diffraction peaks at 25°, 27°, and 32° [50].

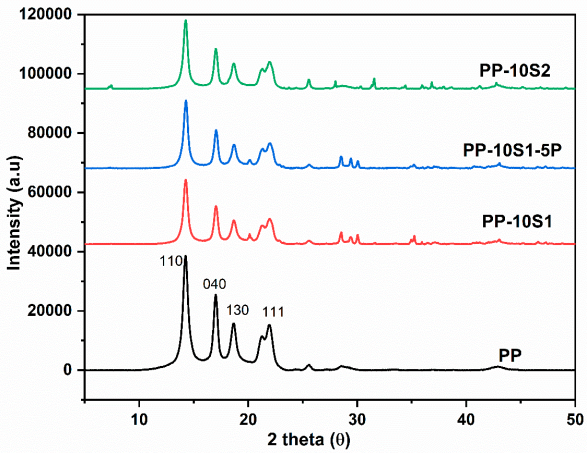

Figure 2. XRD pattern of PP, PP/10S_1, PP/10S_1/5P, and PP/10S_2.

3.3. Thermal Gravimetric Analysis (TGA)

The TGA results collected for PP, PP/S_1, PP/S_2, S_1, and S_2 under an inert atmosphere are shown in Figure 3A–C, respectively. For both S_1 and S_2 composites, the degradation process occurred in a single step and the composite with the highest filler loading have better thermal stability than that of neat PP. The better thermal stability of the composites is because of the fact that the inorganic filler particles (S_1 and S_2) can act as a barrier, slowing down the decomposition process of PP [43]. However, in low filler loading concentrations, the thermal stability decreased. Moreover, the residual weight left at the end of the TGA curve was proportional to the loading percentage of the S_1 and S_2 fillers. Both S_1 and S_2 are inorganic materials and are very much stable as seen from the TGA graph (Figure 3C). The weight loss is very much negligible for both the S_1 and S_2, and on comparing S_1 and S_2; S_2 is found to be slightly more stable than S_1. The S_1 and S_2 are found to be stable until 300 °C and the minor weight loss starts from that temperature, as shown in Figure 3C.

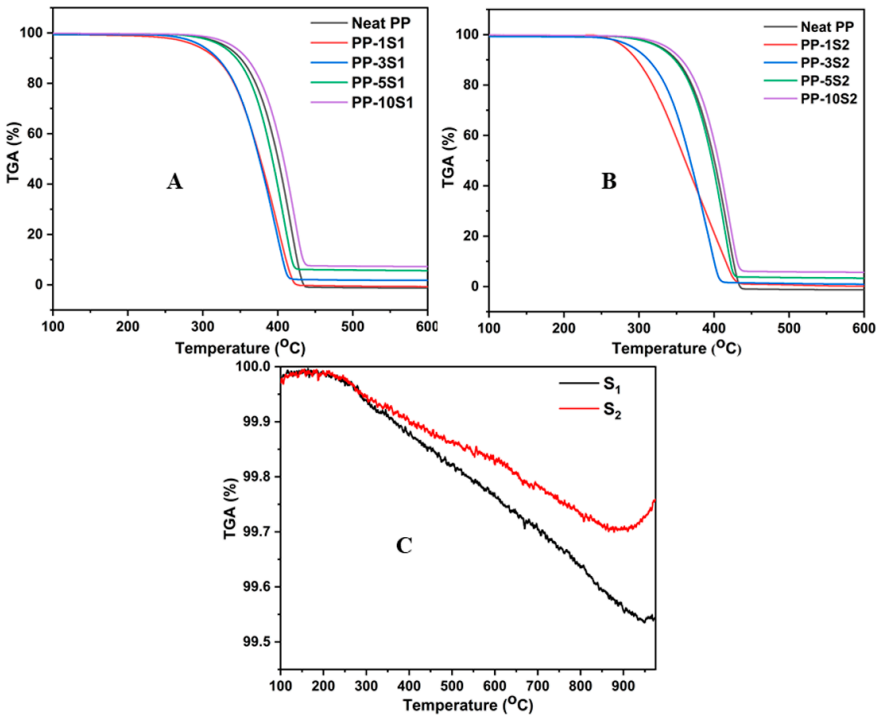

Figure 3. TGA curves of PP/S_1 (**A**), PP/S_2 composites (**B**), S_1 and S_2 (**C**).

3.4. Phosphorescence Emission

The phosphorescence emission spectra of PP/S_1 and PP/S_2 composites are presented in Figures 4 and 5, respectively. The emission spectra were collected at an excitation of 320 nm. As expected, the intensity of emission in the spectra of S_1 and S_2 were higher than that of PP composites because of the opacity and UV resistance of PP. In the PP/S_1 and PP/S_2 composites spectra, the emission intensity increased by increasing the percent loading of both S_1 and S_2. The PP/S_1 composite generated a green emission at 520 nm attributed to the electronic transition of europium divalent ion (Eu^{2+}) in the S_1 phosphors ($4f^6 5d^1$ to $4f^7$) [10,51]; the detailed mechanism of phosphorescence has already been described [52]. The PP/S_2 composites produced a blue emission at 495 nm and the emission intensity increased by increasing the S_2 content (Figure 5). The green (PP/S_1) and blue (PP/S_2) emissions in the dark are shown in Figure 6A,B, respectively.

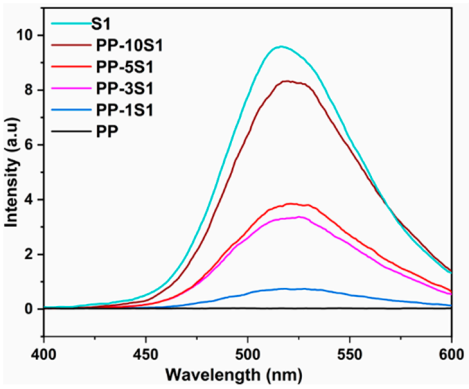

Figure 4. Phosphorescence emissions of S_1 and PP/S_1 composites (excitation wavelength: 320 nm; green emission at 520 nm).

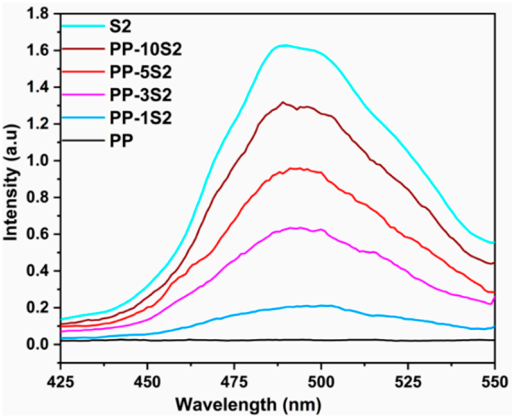

Figure 5. Phosphorescence emissions of S_2 and PP/S_2 composites (excitation wavelength: 320 nm; blue emission at 495 nm).

To investigate the effect of incorporation of plasticizer on the phosphorescence emission, 2.5 and 5 wt.% of plasticizers were added to composite with 10 wt.% of S_1; however, the plasticizer exhibited an adverse effect on the intensity of emissions. The incorporation of the plasticizer in the 10 wt.% S_1 composite decreases the overall phosphorescence emission intensity, as shown in Figure 7. The excitation process in S_1 and S_2 by absorbing UV light may get hindered in the presence of the plasticizer, which is more prone to degradation in UV light [53]. Because of the negative outcome of the plasticizer incorporation on the phosphorescence intensity of the PP/S_1 composites, they were not studied for the PP/S_2 composites.

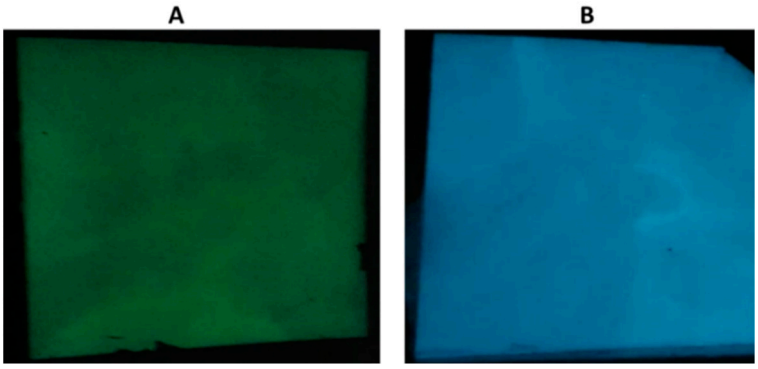

Figure 6. Phosphorescent composites—(**A**) PP/10S_1 in the dark (green emission) and (**B**) PP/10S_2 in the dark (blue emission).

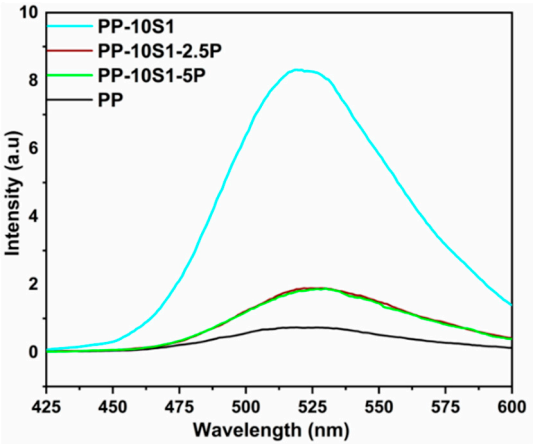

Figure 7. Phosphorescence emission of PP/10S_1 composites with 2.5 and 5 wt.% P plasticizers (excitation wavelength—320 nm; blue emission at 495 nm).

3.5. Mechanical Characteristics of PP/S_1 and PP/S_2 Composites

For practical application purposes, the composites must exhibit suitable physical properties. Therefore, the Izod impact strength and tensile data of the PP with PP/S_1 and PP/S_2 composites were evaluated and are illustrated in Figures 8 and 10, respectively.

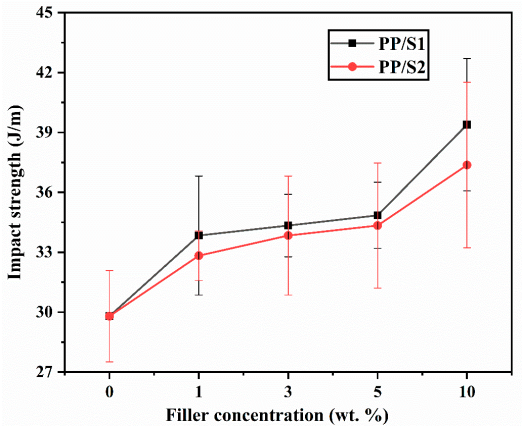

Figure 8. Impact strength of PP/S_1 and PP/S_2 composites.

The impact strength of PP/S_1 and PP/S_2 composites increased gradually by increasing the S_1 and S_2 contents as shown in Figure 8. The PP composites with 10 wt.% filler (S_1 and S_2) showed the highest notch impact strength, which is ~ 32% greater than that for PP.

The increase in the impact strength of the composites is because of the better interfacial adhesion among the PP and fillers (S_1 and S_2), which allows more efficient stress transfer. The distribution of fillers and the increased adhesion between the fillers and PP are visible in the SEM images of the composites with the highest S_1 and S_2 loading of 10 wt.% (Figure 9A,B).

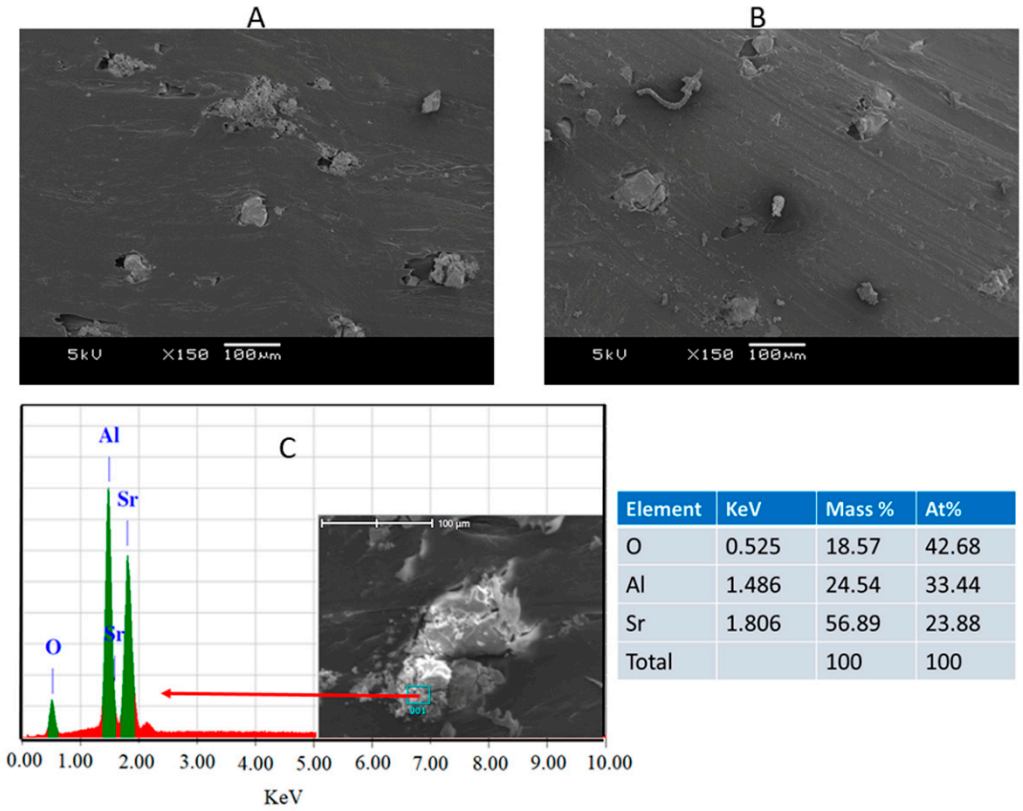

Figure 9. SEM images of PP/10S_1 (**A**) and PP/10S_2 (**B**) composites, and (**C**) SEM-EDS of PP/10S_1.

The tensile properties of PP and PP/S_1 and PP/S_2 composites are presented in Figure 10A,B, respectively. A gradual decrease in TS and tensile TM of the composites can be seen with the increase in the weight content of S_1 and S_2. In the highest filler loading (10 wt.% S_1 and S_2), the TS and TM decreased from 34.5 to 30.5 MPa and 1.1 to 0.94 GPa, respectively. The decrease in the tensile properties of PP/S_1 and PP/S_2 composites by increasing the filler loading can be due to the fact that the presence of inorganic fillers (S_1 and S_2) generally influences the elastic properties of PP because of their intrinsic stiffness and incapability to transfer the applied stress [37]. These observations are in agreement with the decrease in elongation at the yield values for these composites, as shown in Figure 10C. This is because of the decrease in PP ductility in the presence of S_1 and S_2 particles, which decreases the PP chain mobility. The inorganic-polymer composites often cause phase separation due to their incompatibility leading to a reduction in elongation at yield and break [54]. Additionally, the agglomeration of S_1 and S_2 filler, as shown in the SEM images (Figure 9A–C), adversely impacts the tensile modulus values.

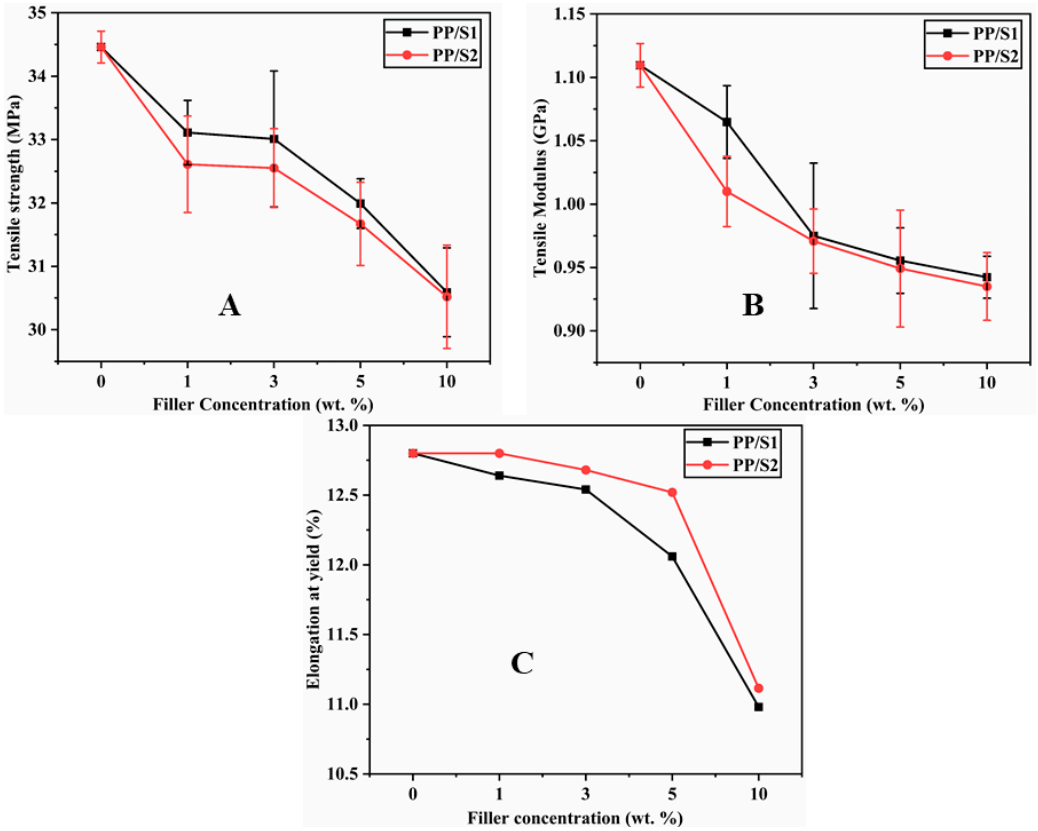

Figure 10. Tensile strength (**A**), tensile modulus (**B**), and elongation at yield (**C**) for PP/S_1 and PP/S_2 composites.

4. Conclusions

In this study, strontium aluminate-based phosphors (S_1 and S_2) were melt-mixed with PP matrix to achieve the long afterglow properties. A long-lasting, PP encapsulated S_1 and S_2 composites with long afterglow properties, which lasts for hours, were obtained. The ATR-FTIR spectra confirmed that the melt-blending process was physical. Moreover, the luminescence spectra of the composite have a major excitation peak at 320 nm and an emission peak at 520 nm (S_1; green) and 495 nm (S_2; blue), respectively. The thermal studies show that the Tc and Tm of PP were not affected by the S_1 and S_2 fillers. However, there was a significant decrease in the crystallinity of the composites with S_2 fillers, owing to the comparatively bulky chemical structure of these fillers. The impact strength of the resultant composites increased with the filler amount, but an adverse effect was witnessed on the TS and TM. These results demonstrated the satisfactory prospects for the formulation of phosphorescence films based on low-cost PP, which has great potential for applications in a new generation of light sources such as traffic signage and emergency signals.

Author Contributions: Conceptualization, A.M.P.; methodology, A.M.P.; investigation, A.A. (Abdullah Alhamidi) and A.Y.E.; writing draft preparation, A.M.P., A.A. (Arfat Anis) and N.S.K.; writing—review and editing, A.M.P., H.S., N.S.K., and A.A. (Arfat Anis); supervision, A.M.P. and S.M.A.-Z.; project administration, A.M.P. All authors have read and agreed to the published version of the manuscript.

Funding: This Project was funded by the National Plan for Science, Technology and Innovation (MAARIFAH), King Abdulaziz City for Science and Technology (13-ADV1044-02).

Institutional Review Board Statement: Not applicable.

Informed Consent Statement: Not Applicable.

Data Availability Statement: The data presented in this study are available on request from the corresponding author.

Acknowledgments: This Project was funded by the National Plan for Science, Technology and Innovation (MAARIFAH), King Abdulaziz City for Science and Technology, Kingdom of Saudi Arabia, Award Number (13-ADV1044-02).

Conflicts of Interest: The authors declare no conflict of interest.

References

1. Harvey, E.N. *A History of Luminescence from the Earliest Times Until 1900*; American Philosophical Society: Philadelphia, PA, USA, 1957. [CrossRef]
2. Liu, X.; Tian, B.; Yu, C.; Tu, B.; Zhao, D. Microwave-assisted solvothermal synthesis of radial ZnS nanoribbons. *Chem. Lett.* **2004**, *33*, 522–523. [CrossRef]
3. Wang, H.; Lu, X.; Zhao, Y.; Wang, C. Preparation and characterization of ZnS:Cu/PVA composite nanofibers via electrospinning. *Mater. Lett.* **2006**, *60*, 2480–2484. [CrossRef]
4. Matsuzawa, T.; Aoki, Y.; Takeuchi, N.; Murayama, Y. A new long phosphorescent phosphor with high brightness, $SrAl_2O_4$:Eu^{2+}, Dy^{3+}. *J. Electrochem. Soc.* **1996**, *143*, 2670–2673. [CrossRef]
5. Palilla, F.C.; Levine, A.K.; Tomkus, M.R. Fluorescent properties of alkaline Earth aluminates of the type MAl_2O_4 activated by divalent europium. *J. Electrochem. Soc.* **1968**, *115*, 642–644. [CrossRef]
6. Nakazawa, T.M.E. Traps in $SrA1_2O_4$: Eu^{2+} phosphor with rare-Earth ion doping. *J. Lumin.* **1997**, *72–74*, 236–237. [CrossRef]
7. Sakai, R.; Katsumata, T.; Komuro, S.; Morikawa, T. Effect of composition on the phosphorescence from $BaAl_2O_4$:Eu^{2+}, Dy^{3+} crystals. *J. Lumin.* **1999**, *85*, 149–154. [CrossRef]
8. Arellano-Tánori, O.; Meléndrez, R.; Pedroza-Montero, M.; Castañeda, B.; Chernov, V.; Yen, W.M.; Barboza-Flores, M. Persistent luminescence dosimetric properties of UV-irradiated $SrAl_2O_4$:Eu^{2+}, Dy^{3+} phosphor. *J. Lumin.* **2008**, *128*, 173–184. [CrossRef]
9. Smets, B.; Rutten, J.; Hoeks, G.; Verlijsdonk, J. $2SrO{\cdot}3Al_2O_3$:Eu^{2+} and 1.29 (Ba, Ca) O, $6Al_2O_3$:Eu^{2+}: Two new blue-emitting phosphors. *J. Electrochem. Soc.* **1989**, *136*, 2119–2123. [CrossRef]
10. Nakazawa, E.; Murazaki, Y.; Saito, S. Mechanism of the persistent phosphorescence in $Sr_4Al_{14}O_{25}$: Eu and $SrAl_2O_4$: Eu codoped with rare Earth ions. *J. Appl. Phys.* **2006**, *100*, 113113. [CrossRef]
11. Zhang, P.; Xu, M.; Zheng, Z.; Liu, L.; Li, L. Synthesis and characterization of europium-doped $Sr_3Al_2O_6$ phosphors by sol–gel technique. *J. Sol Gel Sci. Technol.* **2007**, *43*, 59–64. [CrossRef]
12. Toh, K.; Nagata, S.; Tsuchiya, B.; Shikama, T. Luminescence characteristics of $Sr_4Al_{14}O_{25}$: Eu,Dy under proton irradiation. *Nucl. Instrum. Methods Phys. Res. B* **2006**, *249*, 209–212. [CrossRef]
13. Lu, Y.; Li, Y.; Xiong, Y.; Wang, D.; Yin, Q. $SrAl_2O_4$:Eu^{2+}, Dy^{3+} phosphors derived from a new sol–gel route. *Microelectron. J.* **2004**, *35*, 379–382. [CrossRef]
14. Katsumata, T.; Nabae, T.; Sasajima, K.; Komuro, S.; Morikawa, T. Effects of composition on the long phosphorescent $SrAl_2O_4$:Eu^{2+}, Dy^{3+} phosphor crystals. *J. Electrochem. Soc.* **1997**, *144*, L243–L245. [CrossRef]
15. Nance, J.; Sparks, T.D. From streetlights to phosphors: A review on the visibility of roadway markings. *Prog. Org. Coat.* **2020**, *148*, 105749. [CrossRef]
16. Tan, H.; Wang, T.; Shao, Y.; Yu, C.; Hu, L. Crucial breakthrough of functional persistent luminescence materials for biomedical and information technological applications. *Front. Chem.* **2019**, *7*, 387. [CrossRef]
17. Lin, Y.; Tang, Z.; Zhang, Z. Preparation of long-afterglow Sr_4Al_{14} O_{25}-based luminescent material and its optical properties. *Mater. Lett.* **2001**, *51*, 14–18. [CrossRef]
18. Zheng, R.; Xu, L.; Qin, W.; Chen, J.; Dong, B.; Zhang, L.; Song, H. Electrospinning preparation and photoluminescence properties of $SrAl_2O_4$:Ce^{3+} nanowires. *J. Mater. Sci.* **2011**, *46*, 7517–7524. [CrossRef]
19. Sakirzanovas, S.; Katelnikovas, A.; Dutczak, D.; Kareiva, A.; Jüstel, T. Synthesis and Sm^{2+}/Sm^{3+} doping effects on photoluminescence properties of $Sr_4Al_{14}O_{25}$. *J. Lumin.* **2011**, *131*, 2255–2262. [CrossRef]
20. Kim, S.J.; Won, H.I.; Hayk, N.; Won, C.W.; Jeon, D.Y.; Kirakosyan, A.G. Preparation and characterization of $Sr_4Al_2O_7$:Eu^{3+}, Eu^{2+} phosphors. *Mater. Sci. Eng. B* **2011**, *176*, 1521–1525. [CrossRef]
21. Chang, C.C.; Yang, C.Y.; Lu, C.H. Preparation and photoluminescence properties of $Sr_4Al_{14}O_{25}$:Eu^{2+} phosphors synthesized via the microemulsion route. *J. Mater. Sci. Mater. Electron.* **2013**, *24*, 1458–1462. [CrossRef]
22. Katsumata, T.; Sasajima, K.; Nabae, T.; Komuro, S.; Morikawa, T. Characteristics of strontium aluminate crystals used for long-duration phosphors. *J. Am. Ceram. Soc.* **1998**, *81*, 413–416. [CrossRef]
23. Suriyamurthy, N.; Panigrahi, B.S. Effects of non-stoichiometry and substitution on photoluminescence and afterglow luminescence of $Sr_4Al_{14}O_{25}$:Eu^{2+}, Dy^{3+} phosphor. *J. Lumin.* **2008**, *128*, 1809–1814. [CrossRef]
24. Peng, T.; Huajun, L.; Yang, H.; Yan, C. Synthesis of $SrAl_2O_4$: Eu, Dy phosphor nanometer powders by sol–gel processes and its optical properties. *Mater. Chem. Phys.* **2004**, *85*, 68–72. [CrossRef]

25. Yeşilay Kaya, S.; Karacaoglu, E.; Karasu, B. Effect of Al/Sr ratio on the luminescence properties of $SrAl_2O_4$:Eu^{2+}, Dy^{3+} phosphors. *Ceram. Int.* **2012**, *38*, 3701–3706. [CrossRef]
26. Chen, I.; Chen, T. Effect of host compositions on the afterglow properties of phosphorescent strontium aluminate phosphors derived from the sol–gel method. *J. Mater. Res.* **2001**, *16*, 1293–1300. [CrossRef]
27. Bem, D.B.; Swart, H.C.; Luyt, A.S.; Duvenhage, M.M.; Dejene, F.B. Characterization of luminescent and thermal properties of long afterglow $SrAl_xO_y$: Eu^{2+}, Dy^{3+} phosphor synthesized by combustion method. *Polym. Compos.* **2011**, *32*, 219–226. [CrossRef]
28. Xue, Z.; Deng, S.; Liu, Y. Synthesis and luminescence properties of $SrAl_2O_4$:Eu^{2+}, Dy^{3+} nanosheets. *Phys. B* **2012**, *407*, 3808–3812. [CrossRef]
29. Chang, C.; Yuan, Z.; Mao, D. Eu^{2+} activated long persistent strontium aluminate nano scaled phosphor prepared by precipitation method. *J. Alloys Compd.* **2006**, *415*, 220–224. [CrossRef]
30. Ravichandran, D.; Johnson, S.T.; Erdei, S.; Roy, R.; White, W.B. Crystal chemistry and luminescence of the Eu^{2+}-activated alkaline Earth aluminate phosphors. *Displays* **1999**, *19*, 197–203. [CrossRef]
31. Pathak, P.K.; Kurchania, R. Synthesis and thermoluminescence properties of $SrAl_2O_4$ (EU) phosphor irradiated with cobalt-60, 6 MV and 16 MV photon beams. *Radiat. Phys. Chem.* **2015**, *117*, 48–53. [CrossRef]
32. Dorenbos, P. Mechanism of persistent luminescence in Eu^{2+} and Dy^{3+} codoped aluminate and silicate compounds. *J. Electrochem. Soc.* **2005**, *152*, H107–H110. [CrossRef]
33. Lü, X.; Zhong, M.; Shu, W.; Yu, Q.; Xiong, X.; Wang, R. Alumina encapsulated $SrAl_2O_4$:Eu^{2+}, Dy^{3+} phosphors. *Powder Technol.* **2007**, *177*, 83–86. [CrossRef]
34. Guo, C.; Luan, L.; Huang, D.; Su, Q.; Lv, Y. Study on the stability of phosphor $SrAl_2O_4$:Eu^{2+}, Dy^{3+} in water and method to improve Its moisture resistance. *Mater. Chem. Phys.* **2007**, *106*, 268–272. [CrossRef]
35. Zhu, Y.; Zeng, J.; Li, W.; Xu, L.; Guan, Q.; Liu, Y. Encapsulation of strontium aluminate phosphors to enhance water resistance and luminescence. *Appl. Surf. Sci.* **2009**, *255*, 7580–7585. [CrossRef]
36. Wu, S.; Zhang, S.; Liu, Y.; Yang, J. The organic ligands coordinated long afterglow phosphor. *Mater. Lett.* **2007**, *61*, 3185–3188. [CrossRef]
37. Tian, S.; Wen, J.; Fan, H.; Chen, Y.; Yan, J.; Zhang, P. Sunlight-activated long persistent luminescent polyurethane incorporated with amino-functionalized $SrAl_2O_4$:Eu^{2+}, Dy^{3+} phosphor. *Polym. Int.* **2016**, *65*, 1238–1244. [CrossRef]
38. Bem, D.B.; Luyt, A.S.; Dejene, F.B.; Botha, J.R.; Swart, H.C. Structural, luminescent and thermal properties of blue $SrAl_2O_4$:Eu^{2+}, Dy^{3+} phosphor filled low-density polyethylene composites. *Phys. B* **2009**, *404*, 4504–4508. [CrossRef]
39. Bem, D.B.; Swart, H.C.; Luyt, A.S.; Coetzee, E.; Dejene, F.B. Properties of green $SrAl_2O_4$ phosphor in LDPE and PMMA polymers. *J. Appl. Polym. Sci.* **2010**, *117*, 2635–2640. [CrossRef]
40. Mishra, S.B.; Mishra, A.K.; Luyt, A.S.; Revaprasadu, N.; Hillie, K.T.; vdM Steyn, W.J.; Coetsee, E.; Swart, H.C. Ethylvinyl acetate copolymer-$SrAl_2O_4$: Eu,Dy and $Sr_4Al_{14}O_{25}$:Eu,Dy phosphor-based composites: Preparation and material properties. *J. Appl. Polym. Sci.* **2010**, *115*, 579–587. [CrossRef]
41. Mishra, S.B.; Mishra, A.K.; Revaprasadu, N.; Hillie, K.T.; Steyn, W.V.; Coetsee, E.; Swart, H.C. Strontium aluminate/polymer composites: Morphology, luminescent properties, and durability. *J. Appl. Polym. Sci.* **2009**, *112*, 3347–3354. [CrossRef]
42. Nance, J.; Sparks, T.D. Comparison of coatings for $SrAl_2O_4$:Eu^{2+}, Dy^{3+} powder in waterborne road striping paint under wet conditions. *Prog. Org. Coat.* **2020**, *144*, 105637. [CrossRef]
43. Wan, M.; Jiang, X.; Nie, J.; Cao, Q.; Zheng, W.; Dong, X.; Fan, Z.H.; Zhou, W. Phosphor powders-incorporated polylactic acid polymeric composite used as 3D printing filaments with green luminescence properties. *J. Appl. Polym. Sci.* **2020**, *137*, 48644. [CrossRef]
44. Piramidowicz, R.; Jusza, A.; Lipińska, L.; Gil, M.; Mergo, P. Re^{3+}: $LaAlO_3$ doped luminescent polymer composites. *Opt. Mater.* **2019**, *87*, 35–41. [CrossRef]
45. Barletta, M.; Puopolo, M.; Trovalusci, F.; Vesco, S. High-density polyethylene/$SrAl_2O_4$:Eu^{2+}, Dy^{3+} photoluminescent pigments: Material design, melt processing, and characterization. *Polym. Plast. Technol. Eng.* **2017**, *56*, 400–410. [CrossRef]
46. Paukkeri, R.; Lehtinen, A. Thermal behaviour of polypropylene fractions: 1. influence tacticity mol. weight crystallization melting behaviour. *Polymer* **1993**, *34*, 4075–4082. [CrossRef]
47. Poulose, A.M.; Elnour, A.Y.; Kumar, N.S.; Alhamidi, A.; George, J.; Al-Ghurabi, E.H.; Boumaza, M.; Al-Zahrani, S. Utilization of polyethylene terephthalate waste as a carbon filler in polypropylene matrix: Investigation of mechanical, rheological, and thermal properties. *J. Appl. Polym. Sci.* **2021**, *138*, 50292. [CrossRef]
48. Vidović, E.; Faraguna, F.; Jukić, A. Influence of inorganic fillers on PLA crystallinity and thermal properties. *J. Therm. Anal. Calorim.* **2017**, *127*, 371–380. [CrossRef]
49. Chiu, F.C.; Chu, P.H. Characterization of solution-mixed polypropylene/clay nanocomposites without compatibilizers. *J. Polym. Res.* **2006**, *13*, 73–78. [CrossRef]
50. Luitel, H.N.; Watari, T.; Torikai, T.; Yada, M. Luminescent properties of Cr^{3+} doped $Sr_4Al_{14}O_{25}$: Eu/Dy blue–green and red phosphor. *Opt. Mater.* **2009**, *31*, 1200–1204. [CrossRef]
51. Aitasalo, T.; Hölsä, J.; Jungner, H.; Lastusaari, M.; Niittykoski, J. Mechanisms of persistent luminescence in Eu^{2+}, Re^{3+} doped alkaline Earth aluminates. *J. Lumin.* **2001**, *94–95*, 59–63. [CrossRef]

52. Clabau, F.; Rocquefelte, X.; Jobic, S.; Deniard, P.; Whangbo, M.H.; Garcia, A.; Le Mercier, T. Mechanism of phosphorescence appropriate for the long-lasting phosphors Eu^{2+}-doped $SrAl_2O_4$ with codopants Dy^{3+} and B^{3+}. *Chem. Mater.* **2005**, *17*, 3904–3912. [CrossRef]
53. Das, I.; Gupta, S.K. Polyethylene glycol degradation by UV irradiation. *Indian J. Chem.* **2005**, *44a*, 1355–1358.
54. Mammeri, F.; Bourhis, E.L.; Rozes, L.; Sanchez, C. Mechanical properties of hybrid organic–inorganic materials. *J. Mater. Chem.* **2005**, *15*, 3787–3811. [CrossRef]